ABSTRACT

COMBUSTION OF AEROSOLIZED SPHERICAL ALUMINUM POWDERS AND FLAKES IN AIR

by
Binu Zacharia Eapen

Combustion rates and completeness of aerosolized spherical aluminum powders and flakes are compared using constant volume explosion experiments. The comparison of particles and flake sizes was made based on their specific surface areas determined using the Brunauer-Emmett-Teller (BET) method and respective "BET diameters". It is observed that the rates of pressure rise and rates of flame propagation were higher for aluminum powders with BET diameters of about 2 to 5 μm compared to aluminum flakes for which the BET diameters were under 1 μm. In agreement with the flame propagation rates, the overall completeness of combustion was also higher for aluminum powders compared to flakes. It is suggested that aerosolized flakes could be agglomerated in gas flows more than spherical particles causing their inferior combustion performance.

COMBUSTION OF AEROSOLIZED SPHERICAL ALUMINUM POWDERS AND FLAKES IN AIR

by
Binu Zacharia Eapen

A Thesis
Submitted to the Faculty of
New Jersey Institute of Technology
in Partial Fulfillment of the Requirements for the Degree of
Master of Science in Mechanical Engineering

Department of Mechanical Engineering

January 2004

Approval Page

COMBUSTION OF AEROSOLIZED SPHERICAL ALUMINUM POWDERS AND FLAKES IN AIR

Binu Zacharia Eapen

Dr. Edward L. Dreizin, Thesis Advisor — Date
Associate Professor of Mechanical Engineering, NJIT

Dr. Chao Zhu, Committee Member — Date
Associate Professor of Mechanical Engineering, NJIT

Dr. Boris Khusid, Committee Member — Date
Associate Professor of Mechanical Engineering, NJIT

BIOGRAPHICAL SKETCH

Author: Binu Zacharia Eapen

Degree: Master of Science

Date: January 2004

Undergraduate and Graduate Education:

- Master of Science in Mechanical Engineering,
  New Jersey Institute of Technology, Newark, NJ, 2004

- Bachelor of Technology in Mechanical Engineering,
  Mahatma Gandhi University, Kerala, India, 1999

Major: Mechanical Engineering

Presentations and Publications:

B. Z. Eapen, V. K. Hoffmann, M. Schoenitz, and E. L. Dreizin
"Combustion of Aerosolized Spherical Aluminum Powders and Flakes in Air," Eastern States Section of Combustion Institute Technical Meeting, Penn State University, State College, Pennsylvania, October 2003.

To my parents and Ahalya

ACKNOWLEDGEMENT

I would like to express my sincere gratitude to my advisor, Dr. Edward L. Dreizin. His constant encouragement and support have been invaluable during my time at the micro-gravity research lab. Both on a professional and on a personal level he has greatly contributed to my life as a graduate student.

I would also like to express my appreciation to the distinguished members of the committee: Dr. Chao Zhu and Dr. Boris Khusid. Their valuable discussions and insightful comments have improved the quality of this thesis.

I would like to thank Defense Threat Reduction Agency (DTRA) and New Jersey Commission on Science and Technology for their support throughout the project.

I also wish to thank Dr. Mirko Schoenitz for his valuable guidance during the project, and last but not least Vern Hoffmann and Steven Jones for their continuous support and guidance throughout the project.

TABLE OF CONTENTS

LIST OF TABLES

LIST OF FIGURES

CHAPTER 1

INTRODUCTION

Aluminum powders are widely used as additives in energetic formulations for propellants, explosives, and pyrotechnics. Particle size and surface morphology are important parameters affecting the rate of combustion of metal additives as well as hydrodynamic particle behavior in the ignition zone and flame area. A number of recent investigations deal with an accelerated burn rate that is possible to achieve using reduced particle sizes and, ultimately, nano-sized aluminum particles, e.g., (Mench et al., 1998, Pranda et al., 2000) produced using state of the art technologies. At the same time, in many practical applications, e.g., in pyrotechnic formulations, aluminum flakes that are readily available commercially are used instead of regular powders. It is generally thought that because of the high specific surface of flakes, they are easier ignited than spherical or spheroid particles of similar mass. An accelerated ignition should result in an acceleration of the overall burn rate of aluminum flakes as compared to regular powders. At the same time, gas dynamics of the flakes should be remarkably different from that of regular powders, which could be important for combustion in multiphase systems. We were unable to find in the literature systematic comparisons of ignition and combustion behaviors of aluminum flakes versus spherical or other "3-dimensional" aluminum particles. Therefore, no guidance is currently available for selection of either regular aluminum powders or flakes as a fuel or fuel additive for applications in explosives, propellants, or incendiaries. Current interest in comparing combustion parameters of aluminum powders and flakes is stimulated, in particular, by development

of fuel-air explosives and thermobaric explosives for which metal aerosol serves as a fuel and air as an oxidizer. Therefore, combustion rates of aerosolized spherical aluminum powders (referred below simply as "powders") and flakes in air are compared in this work. A constant volume explosion experimental technique is used to assess the burn rates based on the measured rates of pressure rise. In addition, combustion products are collected and analyzed.

CHAPTER 2

MATERIALS

A set of commercially available aluminum powders with particle sizes in the 1- 50 μm range was compared to a set of commercially available aluminum flakes. Aluminum powders were acquired from Alfa Aesar, Atlantic Equipment Engineers, and Toyal America. Representative Scanning Electron Microscope (SEM) images of aluminum particles are shown in Figure 2.1. One can see that most of the particles have spherical or nearly spherical shapes. Particles by Atlantic Equipment Engineers are somewhat less spherical than other powders, however, the difference in the shape does not appear to be significant. Particle sizes were measured by Low Angle Laser Light Scattering (LALLS) using a Coulter LS 230 Enhanced Laser Diffraction particle size analyzer. The resulting size distributions are shown in Figure 2.2. Respective mean particle diameters based on both sample volume and surface area are shown in Table 2.1. Particle sizes were also measured using the SEM images and BET isotherm (multipoint analysis, using a High Speed Gas Sorption Analyzer, NOVA 3000.) and are tabulated as in Table 2.1.

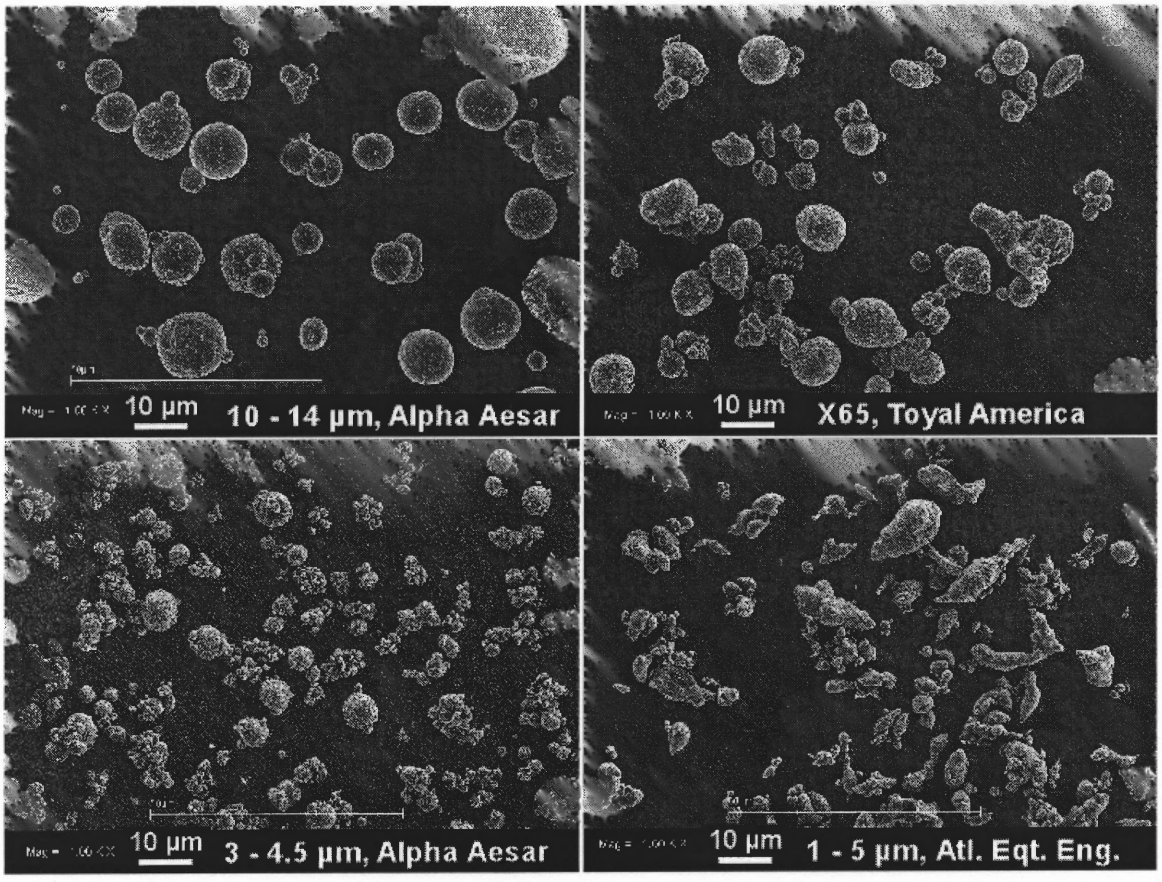

Figure 2.1: Scanning Electron Microscope Images Of Aluminum Powders Used.

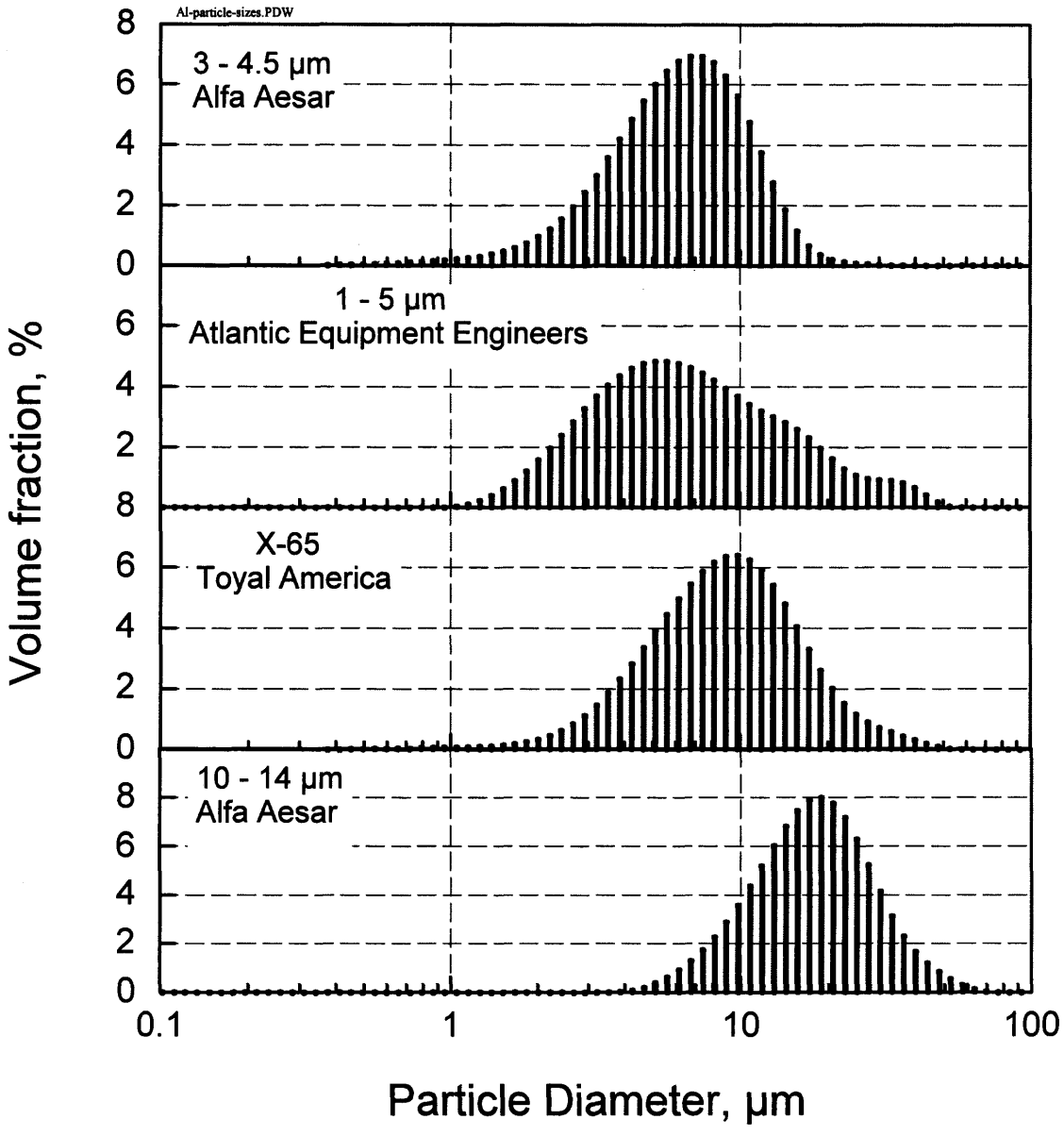

Figure 2.2: Size Distributions For The Aluminum Powders Obtained Using Low Angle Laser Light Scattering (LALLS).

The flakes were acquired from Iowa Pyro Supply, representative SEM images are shown in Figure 2.3. To initially assess the reference particle size for the flakes, the SEM images were analyzed so that typical dimensions were determined for flakes positioned parallel to the image plane. These dimensions measured from the SEM images generally

agreed with those implied by the mesh sizes specified by the flake suppliers. In several images, flakes positioned normally to the image plane were observed as shown for example in Figure 2.4. Several measurements of the flake thickness were made. The observed thickness varied from 20 nm to 200 nm.

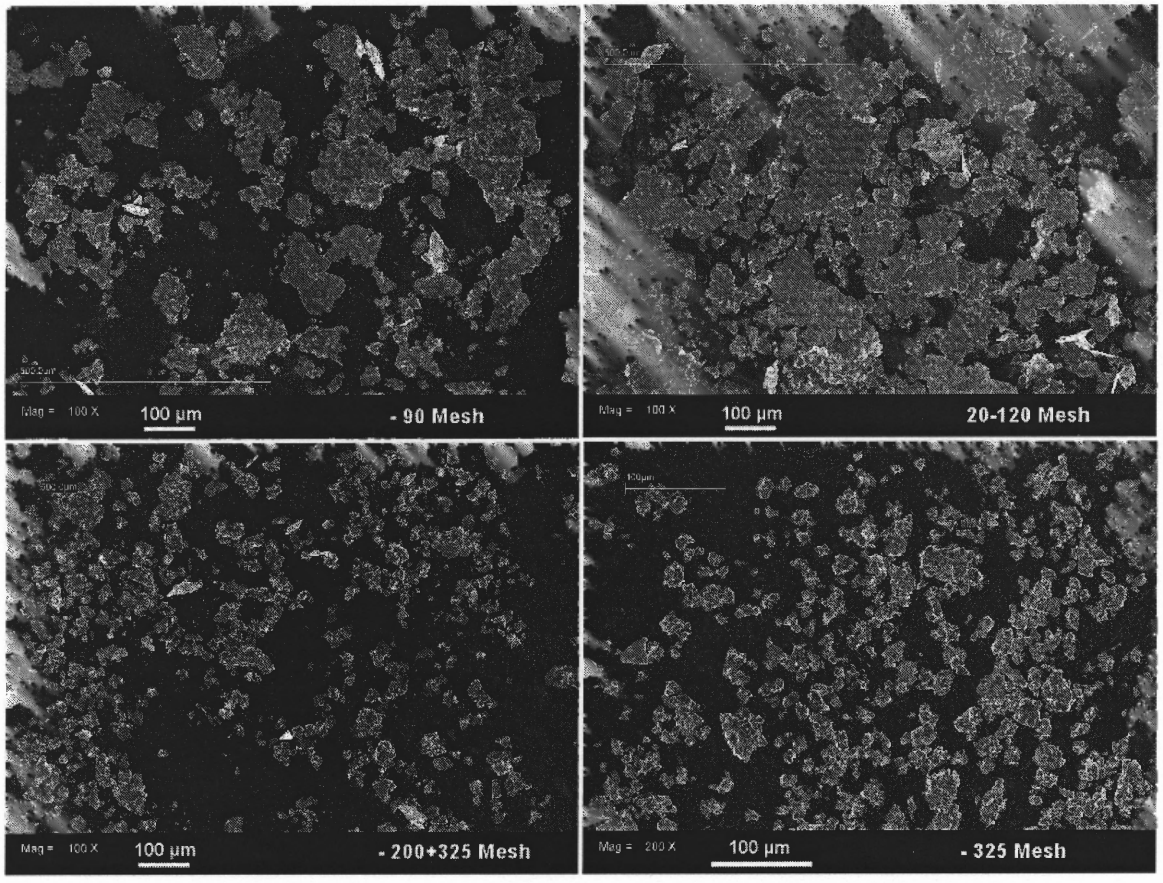

Figure 2.3: Scanning Electron Microscope Images Of Aluminum Flakes Used.

Specific surface area of the flakes, A, was determined by nitrogen absorption employing the BET isotherm (multipoint analysis, using a High Speed Gas Sorption Analyzer, NOVA 3000.) Based on these measurements, equivalent BET diameters for the flakes were estimated as $d_{BET}=6/(\rho A)$ where ρ is the aluminum density, 2.7 g/cm^3 (Winter, 2003).

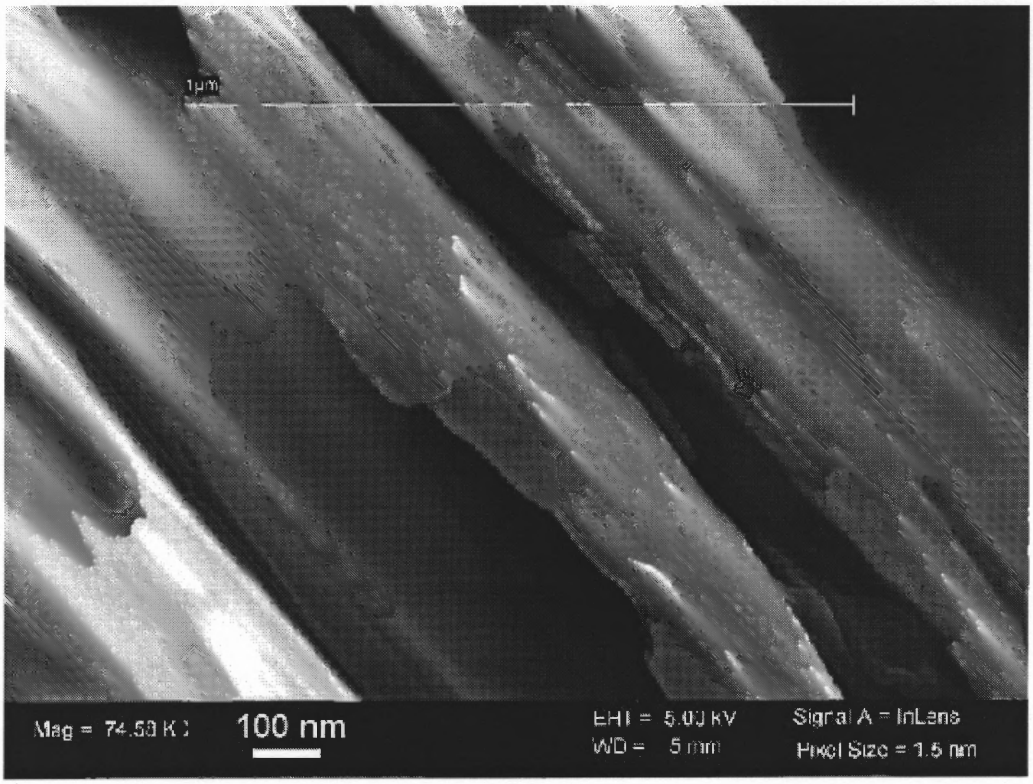

Figure 2.4: High Magnification, SEM Image Of Aluminum Flakes Showing Their Thickness.

To provide a fair comparison between the combustion behavior of flakes and particles, specific surface areas of particles were also measured using a BET isotherm and equivalent BET diameters were computed and shown in Table 2.1. These BET diameters for both flakes and powders were used as a reference size to compare the measured combustion parameters. Note that the BET equivalent diameters for the flakes are about an order of magnitude smaller than those of powders. This is generally consistent with the very small flake thickness as observed using SEM, *cf.* Figure 2.4.

Table 2.1: Particle and Flake Sizes Determined Using SEM Images, LALLS and BET

Type of Al		ID per manufacturer	Mean diameter ,μm from SEM images	Mean diameter, μm based on volume distribution by LALLS	Mean diameter, μm based on area distribution by LALLS	Specific Surface Area, m^2/g by BET	Equivalent BET diameter, μm
FLAKES	IOWA PYRO SUPPY	-325 mesh	20.54	N/A	N/A	7.75	0.30
	IOWA PYRO SUPPY	200+325 mesh	26.73	N/A	N/A	4.78	0.47
	IOWA PYRO SUPPY	20-120 mesh	70.71	N/A	N/A	3.20	0.71
	IOWA PYRO SUPPY	-90 mesh	88.53	N/A	N/A	3.16	0.72
POWDERS	ALFA AESAR	3-4.5 μm	11.42	7.18	5.20	0.013969	1.93
	ATLANTIC EQUIPMENT ENGINEERS	1-5 μm	11.39	9.38	5.39	0.009465	2.81
	TOYAL AMERICA	X-65	24.26	10.87	7.40	0.006129	4.92
	ALFA AESAR	10-14 μm	17.91	20.33	16.28	0.003351	5.41

CHAPTER 3

EXPERIMENTAL SETUP AND METHODOLOGY

3.1 EXPERIMENTAL SETUP COMPONENTS

The schematic presentation for the connections made to the experimental setup is shown in Figure 3.1.1.

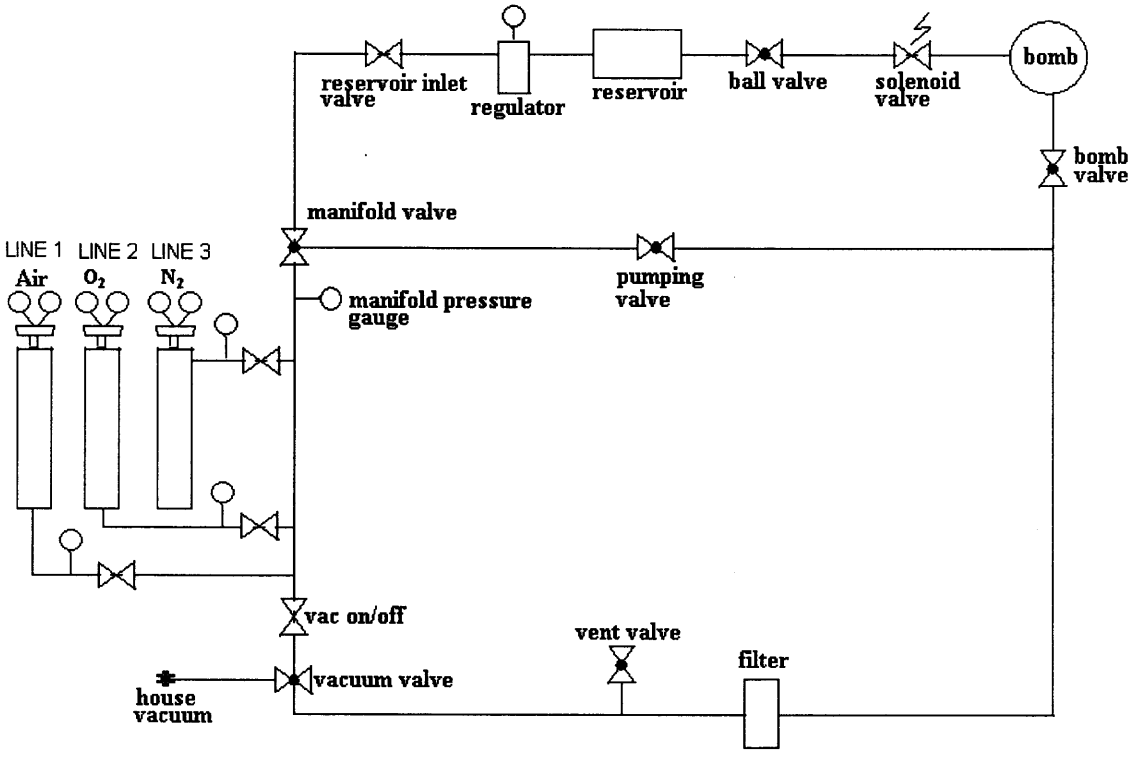

Figure 3.1.1: Detailed Explanation for the Experimental Setup.

The different components for the experimental setup are described below.

Reservoir: A pressure vessel manufactured in accordance with the American Society of Mechanical Engineers' (ASME) serves as the reservoir to hold compressed gas; supplied from a compressed gas cylinder .The volume of the reservoir is seven liters. A pressure transducer manufactured my ASHCROFT connected to the reservoir records the pressure

trace at Channel C of the data acquisition board.

Figure 3.1.2: Experimental Setup.

Constant Volume Vessel or Bomb: The volume of bomb is 9.2 liters. It is built of two halves held together by clamps designed after the constant volume explosion tests by US Bureau of Mines. A pressure transducer manufactured by SCHAEVITZ, fitted with the bomb records the pressure trace at Channel A of the data acquisition board. The two arms in the bomb hold the igniter wire.

Air Filter: After the experiment the gases released to the atmosphere pass through the air filter. It prevents exposing of burnt particles into the atmosphere. The air filter is manufactured by Graver Technologies, LKV 110-005FT-N. The maximum pressure for

the air filter is 150 psi.

Ball Valve: Ball valve is positioned between the reservoir and the solenoid valve. The ball valve is a controlling measure for the amount of air to be passed from the reservoir. The manufacturer for the ball valve was Milwaukee Valve Company, Inc.

Solenoid Valve: Solenoid valve is set to open for 0.2 sec to allow the air from the reservoir to be blown inside the bomb apparatus. The manufacturer is the U L Valves, and the model is S211 GF02 K4DG1. The maximum pressure range for the solenoid valve is 250 psi.

Reservoir Inlet Valve and Regulator: It regulates the amount of compressed air to be filled in the reservoir, which is calibrated to 75 psig. The reservoir inlet valve is manufactured by Whitey Toggle Valves and the regulator by Masoneilan Regulators Co. The regulator is made of aluminum and has the pressure range of 5-100 psi.

Manifold Valve: Manifold valve is the controlling valve for the flow of oxidizer to the bomb or reservoir. It's a two-way valve manufactured by Parker Industries.

Bomb Valve: Bomb valve is the control point in the bomb through which the vacuuming operation is done after which it is closed. Also after the experiment the valve is opened to release the burnt gas to the air filter. Bomb valve is manufactured by Valpres.

Pumping Valve: Pumping valve allows the direction to be set whether the bomb is to be vacuumed or to be filled with any oxidizer. Pumping valve is manufactured by Whitey Toggle Valves.

Vent Valve: Vent valve is used to release the burnt gases after it has been passed through the air filter. Vent valve is manufactured by Whitey Toggle Valves.

Pressure Gauges: Each of the oxidizer cylinders has separate pressure gauges to show the pressure readings, manufactured by Matheson Gas Products. Manifold pressure gauge shows the oxidizer pressure available at the manifold. Vacuum pressure gauge shows the pressure at which house vacuum is supplied. Manifold pressure gauge is manufactured by Ashcroft industries and the vacuum pressure gauge is manufactured by United Instrument.

Auto Transformer: Autotransformer regulates the voltage supplied for the igniter wire. The transformer is manufactured by The Superior Electric Co and the type is 3PN116B. The output voltage range is 0-140 V.

DC Power Supply: Both the pressure transducers are connected to two separate DC power supply at 15 VDC, manufactured by OTE DC POWER SUPPLY. The model is HY3003.

Data Acquisition Board: The data acquisition board used to record the pressure traces is manufactured by Rapid Systems. It has four channels connected to it with Channel A recording the pressure trace in the constant volume vessel, Channel B recording the trigger pulse, Channel C recording the pressure trace from the reservoir and Channel D recording the ignition pulse.

Pressure Transducer: Pressure transducer connected to the constant volume vessel records the pressure trace on channel A and the transducer connected to the reservoir records the trace on channel C. The transducer at constant volume vessel is manufactured by SCHAEVITZ, model- PS10073-0005-250PA. It has the range of 0-250 psiA. The transducer connected to the reservoir manufactured my ASHCROFT and it has the range of 0-150 psiG.

File Nomenclature: The pressure traces recorded are saved as generic ASCII format (*.ASCII) and also in binary format (*.DAT). The file names follow a simple nomenclature. For Ex: a file named 0220R065 has the first four characters as the month and the date of experiment and R065 is the run number.

3.2 EXPERIMENTAL PROCEDURE

A schematic presentation for the experimental setup is shown below in Figure 3.2.1.

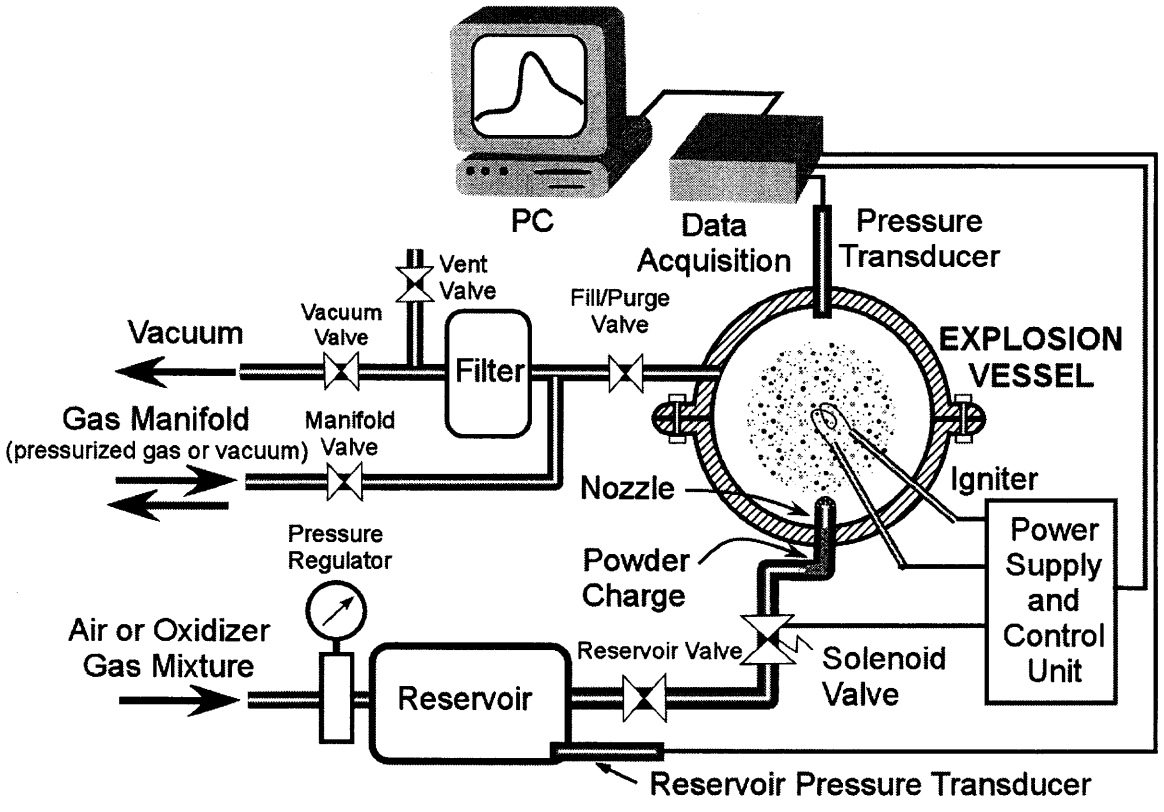

Figure 3.2.1: Experimental Apparatus.

Before starting the experiment, the bomb has to be cleaned. First, the upper lid of the bomb is cleaned with a brush for the remaining powders or products from the last experiment. After brushing, a vacuum cleaner is used to clean up the bomb. Next a paper towel is wet with ethanol or acetone and the interior of the upper lid is wiped out. The nozzle (inside and outside) and the O-ring (used between the bomb halves) should also be cleaned with ethanol. Close the safety door and lock it. The reservoir is filled with compressed air to about 75 psiG, which should be enough for puffing the bomb about

four times. The bomb is puffed without the upper lid. The number of puffs depends on the amount of powder left in the powder reservoir (usually 4 is enough). Finally the dust in the lower lid of the bomb is wiped and cleaned with ethanol.

Next step is to make the igniter wire. Cut off 5 cm (igniter length can be varied according to the voltage needed to be supplied) of a tungsten wire (manufactured by Alpha Aesar) and make a coil of it. The diameter of the tungsten igniter wire is 0.2 mm. Fix it between he electrical supply rods. Coat the igniter wire with Liquid Electrical Tape. The coating need not be a heavy coating but it should cover all parts of the igniter wire. Allow it to dry up (10 min). Clean the sample bottle and the spoon, which is used to take powder. Weigh the required amount of powder, and load it inside the bomb. Attach the nozzle .Put the washer (O-ring) in before the bomb lid is placed over. Fasten the clamps. For fastening the bomb, place the upper half so that the alignment marks on both the halves coincide. Connect the electrical supply wire to the bomb. Change the system settings as explained below for pumping the bomb out.

For evacuating the bomb, change the PC settings as listed in Table 3.2.1. For pumping the bomb, the pressure is monitored by running the data acquisition continuously.

Table 3.2.1: Gain and Software Settings During Pumping the Vessel and Running the Experiment.

SETTINGS	EVACUATION				EXPERIMENT			
GAIN AT CHANNELS	A	B	C	D	A	B	C	D
	0.512	0.512	5.12	2.56	12.8	12.8	5.12	2.56
TRIGGER	AUTOMATIC AND CONTINOUS				AUTOMATIC AND SINGLE SHOT			
SAMPLING RATE	500 KHz				5KHz			
AMPLITUDE RANGE	0.071 V				10.000 V			
AMPLITUDE POSITION	0.196 V				5.000 V			
DISPLAY MODE	OVERLAYED				OVERLAYED			
TIME POSITION	0.000				0.000			
CHANNEL SELECTION	A				ALL FOUR CHANNELS			
COMPRESSION RATIO	1:50				1:50			

By pressing the spacebar data acquisition starts. The pumping of the bomb should continue until the voltage is at 0.196 V. Turn the vacuum valve (VALVE 1) slowly toward the BOMB (Figure 3.2.3: panel diagram). You can see the voltage signal from the pressure transducer decreasing. (Figure 3.2.2). Turn the VALVE 1 back to normal position to stop the trace at 0.196V, which corresponds to 4.87 psiA {calibration is defined by the formula pressure (psiA) = 24.996*voltage (V) -0.0242}. Press the spacebar to stop data acquisition and close the bomb valve.

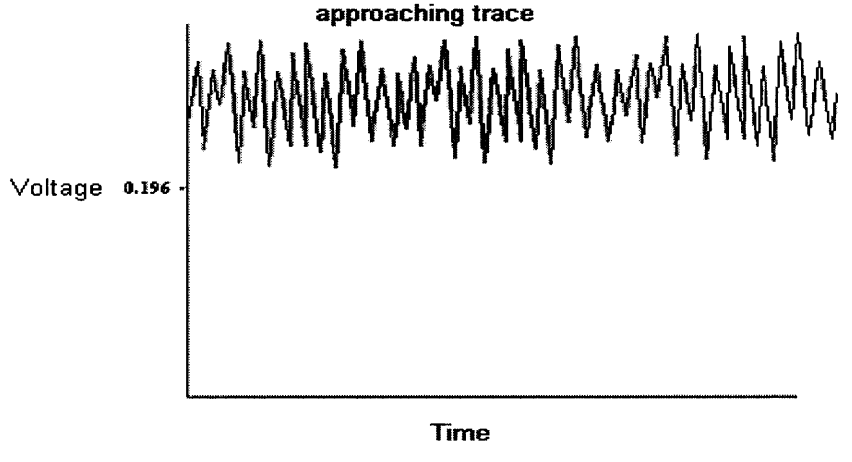

Figure 3.2.2: Approaching Trace During Vacuuming the Vessel.

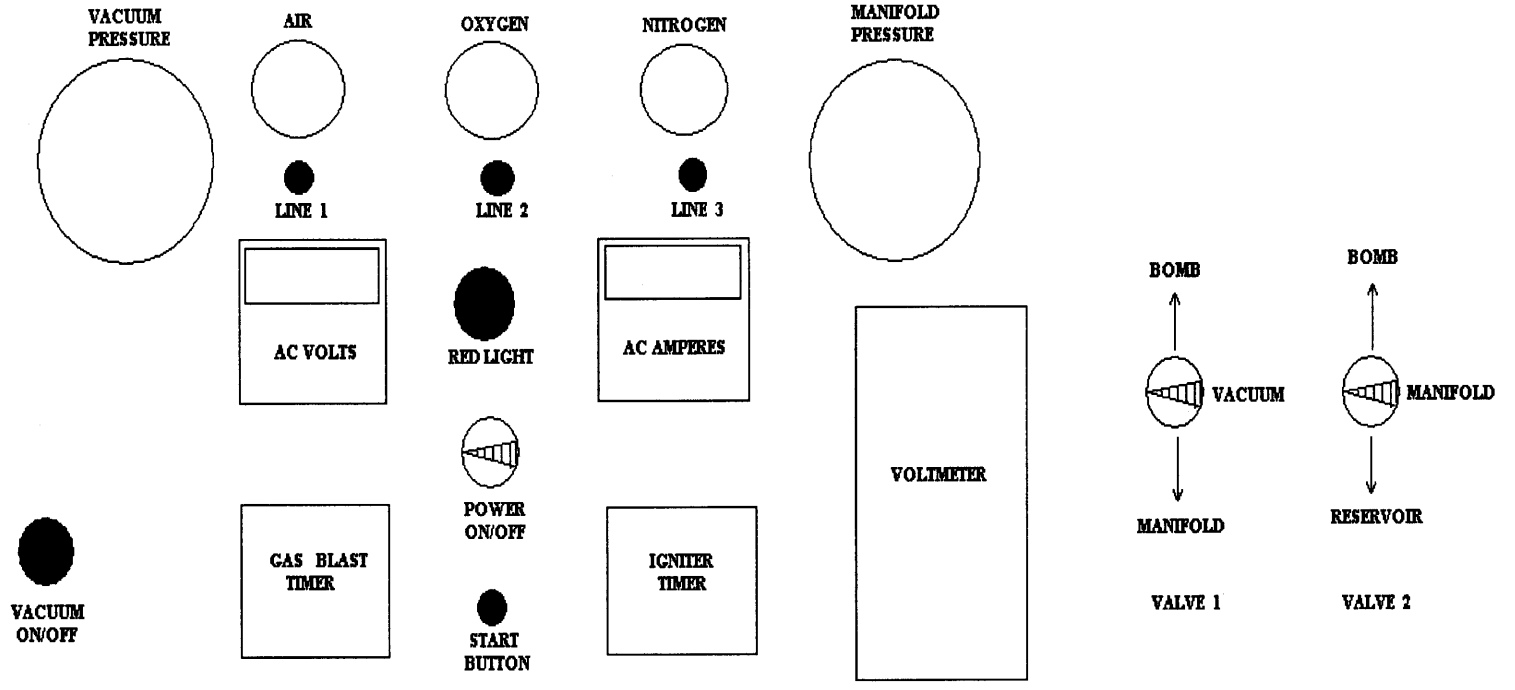

Figure 3.2.3: Panel Diagram

Change the settings for running the experiment as shown in Table 3.2.1.The settings as tabulated are first changed. Press the spacebar to run the data acquisition and note down the initial pressure inside the bomb, which is pre-set to be one third of the atmosphere. Note the reading.

Change the channel selection to select all the four channels. The reservoir is filled with compressed air supplied through Line 1 (Figure 3.2.3: PANEL DIAGRAM). Fill the reservoir with 75 psig compressed air by first turning the VALVE-2 towards the reservoir and then slowly opening LINE-1. Close the LINE-1, as the manifold pressure gauge shows 75 psi.

Check the clamps on the bomb. Check if the ball valve is open. Attach the supply wire to the copper electrodes (Figure 3.2.4). Pull the door down and close it. Set the supply voltage from the transformer according to the length of the igniter wire as shown below in Table 3.2.2. A voltmeter is attached to the capacitors to show the voltage supplied.

Table 3.2.2: Voltage To Be Supplied for the Igniter Wire Based On The Length Used

Igniter wire material	Tungsten		
Supplier	ALPHA AESAR		
Diameter of wire	0.2 mm		
Length of igniter wire (cm)	5	10	15
Time until melting (ms)	60	50	73
Voltage (auto-transformer output)	40.7	71.2	85.5

[The voltage required for a particular length of igniter wire was determined by testing different lengths of the igniter wires at different voltages and finding the time it took to heat the wire]

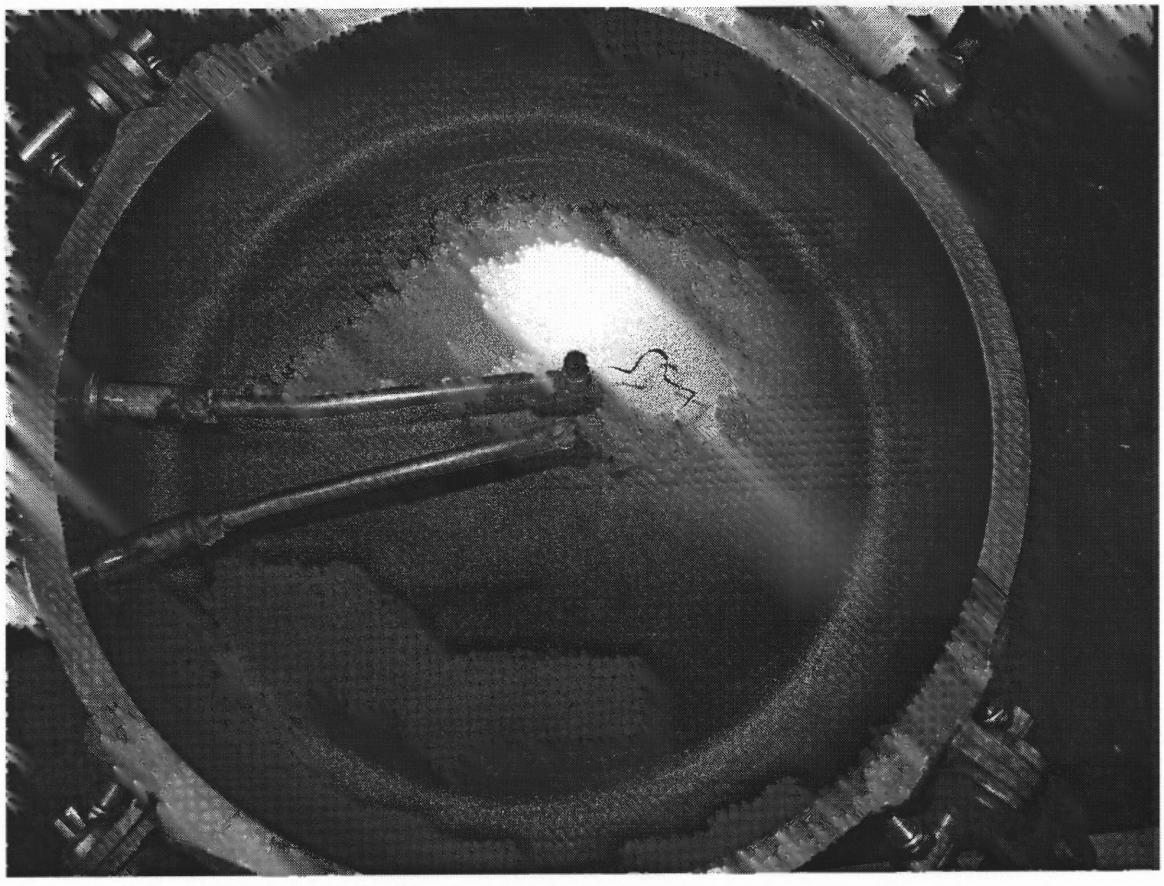

Figure 3.2.4: Igniter Wire Connected to Electrodes.

Turn the transformer supply to approximately 36 VAC so as the voltmeter connected to the capacitors shows the required voltage (VDC) for the 5 cm igniter wire. Turn on the POWER ON/OFF switch to energize the time relays controlling the experiment and observe a red light glowing.

One needs to press the spacebar to start the data acquisition and very quickly (within 0.5 sec) the START BUTTON. After observing the pressure traces on screen, save the file for all channels. Save the files for both binary and generic ASCII format as explained in the beginning. To record the final pressure in the bomb, press the spacebar again at least after one minute of doing the experiment. Save the trace for final pressure with all four channels selected, also in both binary and generic ASCII format.

After the experiment, open the bomb valve to release the gases inside the vessel through the AIR FILTER. Vent the bomb 3 to 4 times so as to release all the burnt gases. Wait for 5 minutes before opening the bomb. Before opening remove the electrical supply wire from the bomb. Collect the sample from the bomb and store it in an airtight plastic bag. Label it with the experiment run number and the powder used.

Repeat the cleaning of the constant volume vessel. The vessel is wiped with ethanol so as to remove the burnt products that are stuck to the surface of the vessel. Remove the nozzle. Put the lid back over the bomb and clamp it. Pull down the door and lock it. Press the START BUTTON so that it's puffed once. Wait for some time for the residual powder to settle down (3 to 4 minutes). Vent the bomb to release the high-pressured air inside by opening the BOMB VALVE slowly. Remove the lid. Use a brush to wipe down the powder and then collect it using a paper. Clean the sample bottle before collecting the residual powder in it. Weigh the powder and enter the record in the lab notebook. Collect the residual powder in an airtight plastic bag and label it with the run number and 'RESIDUAL' written on it.

CHAPTER 4
ANALYSIS

4.1 Terminology

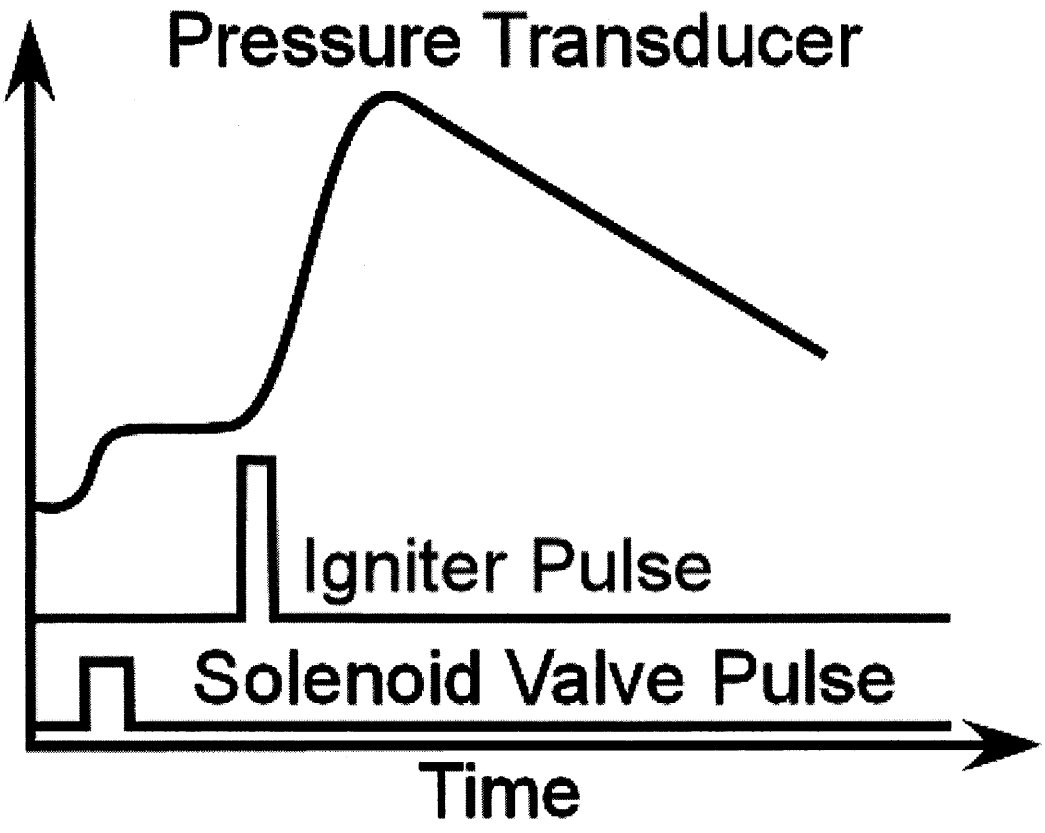

Figure 4.1.1: Typical Real Time Trace Recorded in Different Channels.

A typical trace is showed in Figure 4.1.1, which shows the traces recorded by channels for pressure rise in the vessel. The solenoid valve pulse trace shows the time when the gas blast occurred for the oxidizer to enter the vessel. The igniter pulse trace shows the time for ignition duration.

Following is terminology used to describe traces, recorded pressure changes during the experiment, and time taken to reach the maximum pressure inside the vessel.

1) t_0 = time when the gas blast started.

The time when the gas blast started after the triggering of the experiment takes place.

2) tign = time when the ignition started (t_0 + 0.5 sec).

The ignition duration for the tungsten igniter depends on the length of the igniter wire. [explained in the experimental setup].

3) t-pmax = time at Pmax.

The time when maximum pressure was reached during the experiment.

4) Time to Pmax = t-pmax – tign.

Time it took to reach the maximum pressure (Pmax) after the ignition started.

5) P_0 = pressure inside the bomb after it was pumped out.

P_0 is calculated by taking average of the pressure between t = 0 to t = to.

6) Pi = initial pressure i.e. after the gas blast.

Pi is calculated by taking average between the point when gas blast ends and the point where tign starts.

7) Pmax = maximum pressure

Pmax is calculated by taking he maximum of the 20,000 points used for the sampling rate.

8) Pf = final pressure in the bomb after the experiment.

Final pressure inside the bomb is calculated by taking average pressure for all the points.

9) Effective mass = mass loaded – residual powder

Where, residual powder is the mass collected after the experiment. Effective mass is the actual amount of powder actually dispersed through the nozzle.

10) Tmax = maximum temperature in Celsius

$$\frac{Pi*V}{R*Troom} = \frac{Pmax*V}{R*Tmax}$$

$$Tmax = \frac{Troom*Pmax}{Pi}$$

11) dp/dt avg = average rate of pressure rise in the vessel

12) dp/dt max = maximum rate of pressure rise in the vessel

13) Pi/Pf ratio

The ratio Pi/Pf shows the completeness of the reaction or the usage of the oxidizer in the reaction.

14) t-dp/dtmax = time when the max rate of pressure rise was reached.

All the data collected according to the terminology above are processed using Microsoft Excel where a MS Excel macro is used. The macro is programmed to calculate to take the averages, slope etc.

4.2 Data Processing

The equivalence ratio, Ψ, was computed for each run using the amount of oxygen in the vessel prior to explosion based on the respective experimental pressure in the vessel, and the loaded powder mass corrected by the experimentally determined amount of residual powder. Each recorded pressure curve was time differentiated and the value of the maximum rate of pressure rise, dP/dt_{max} was found. The experimental values of dP/dt_{max} were presented for each material type (different size aluminum powders and flakes) as a function of the experimental equivalence ratio and a linear fit was found for each material. To compare materials to one another, the effect of somewhat different equivalence ratios in different runs should be minimized. Using the found linear fit for each material type, the values of dP/dt_{max} corresponding to the equivalence ratio of 1 were identified for each material (Figure 4.2.1 and 4.2.2). The error of such $dP/dt_{max}(\Psi=1)$ was estimated as a standard deviation of the experimental $dP/dt_{max}(\Psi)$ values from those implied by the produced linear fit at all the respective equivalence ratios. Characterizing each powder with its respective values of dP/dt_{max} found at $\Psi=1$ enabled direct comparisons of the maximum rates of pressure rise, and, therefore, the rates of flame propagation, for different material types.

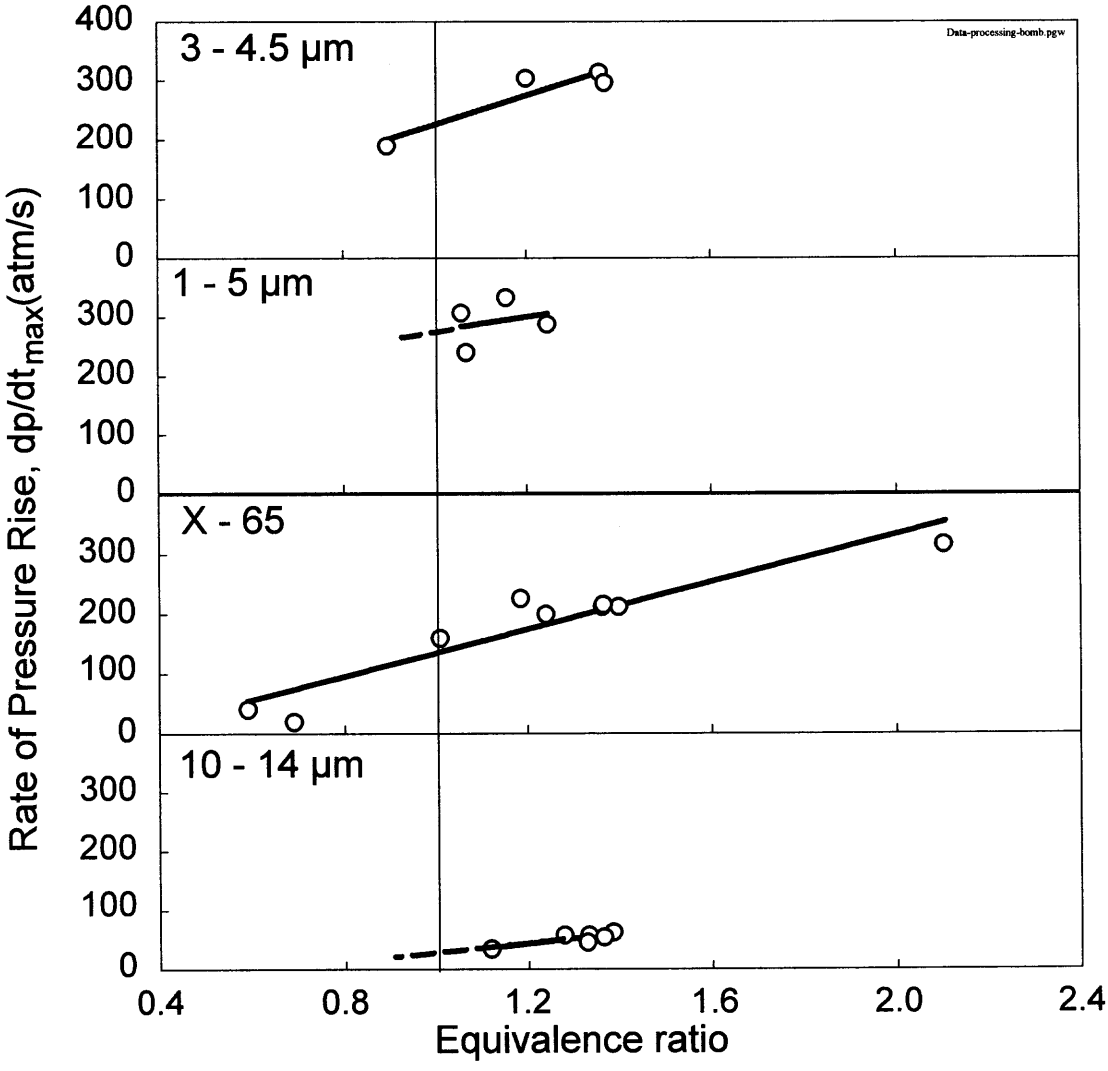

Figure 4.2.1: Comparison of Aluminum Powders.

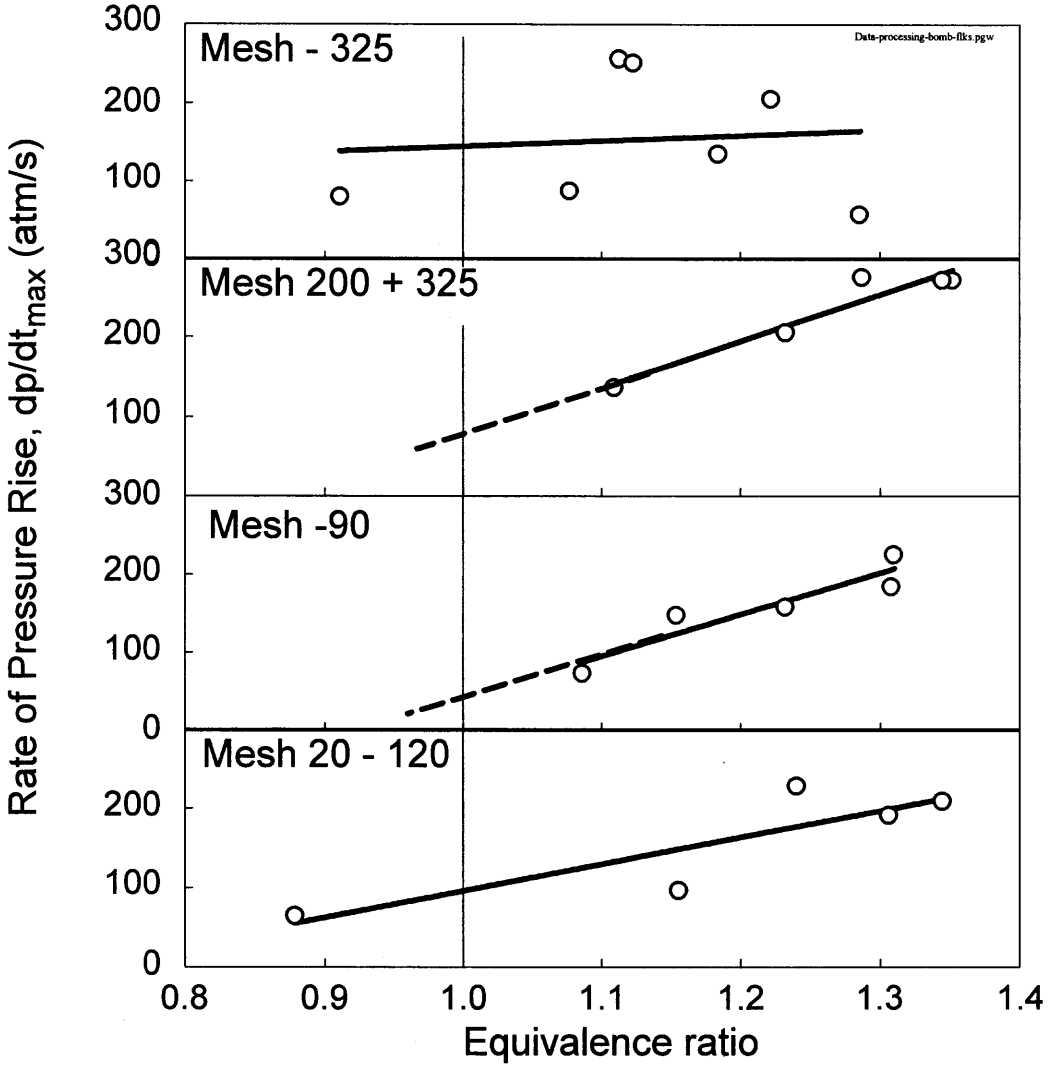

Figure 4.2.2: Comparison of Aluminum Flakes.

4.3 Equivalence Ratio Calculation

$$\text{Equivalence ratio} = \frac{(\text{Air/Fuel})st}{(\text{Air/Fuel})}$$

Reaction

$4Al + 3O_2 = 2Al_2O_3$

Stoichiometry

$$(\text{Air/Fuel})st = \frac{3}{4} = 0.75$$

For (Air/Fuel),

Fuel

$$\frac{\text{Effective mass (g)}}{\text{Molar wt of Al}}$$

Air

$$\frac{\text{Volume of bomb (std liters of air)* Initial Pressure (Pi psiA)}}{1 \text{ atm}}$$

$$\frac{9.2 * 15}{14.7} = 9.38 \text{ std liters of air}$$

[For example in above calculations, initial pressure, Pi =15 psiA]

Oxygen occupies 20.95 % of volume: 20.95 % of 9.38 = 1.96 standard liters of Oxygen.

Number of moles per liter of oxygen = 22.414 liters/mole

Therefore, Air = $\frac{1.96 \text{ liters}}{22.414 \text{ liters/mole}}$

= 0.087 moles

Equivalence ratio less than 1 shows a fuel lean burning mixture and more than 1 shows a fuel rich burning of the mixture.

CHAPTER 5

RESULTS AND DISCUSSION

5.1 Results

The Table 5.1.1 and Table 5.1.2 shows the parameters recorded during the experiment for the spherical powders and flakes. The respective powders and flakes being tested are listed in accordance with their run numbers. The amount of material loaded in the constant volume vessel for the testing is varied to observe the dependence of the powder mass and the equivalence ratio. The length of the igniter wire used was 5 cm.

From the general data collection sheet (Table 5.1.1 and Table 5.1.2), the initial pressure (Pi) for most of the tests for spherical powders and flakes is approximately same. For few of the experiments there is a variation in the initial pressures due to leak through the vessel before the ignition.

Table 5.1.1: General Data Collection Sheet For Spherical Powders

RUN NO	POWDER	MASS (gms)	FUSE (cm)	P_O (psia)	P_i (psia)	P_{max} (psia)	t@ P_{max} (sec)	t_o (sec)	t_{ign}Dur (sec)	t to P_{max} (sec)	Pfinal (psiA)	Effective mass(gms)	dP/dt (avg)	T_{max}	dP/dt max
OCT4R014	AL,X-65	4.65	5	4.99	19.97	143.7	1.09	0.44	N/A	0.145	N/A	N/A	53.51	2138	159.90
OCT7R019	AL,X-65	2.65	5	4.23	19.39	112.5	1.34	0.42	N/A	0.382	N/A	2.36	15.81	1657	40.41
OCT7R018	AL,X-65	3.00	5	4.21	18.78	92.5	1.63	0.43	N/A	0.72	N/A	2.67	6.63	1380	19.33
1120R049	AL,X-65	4.65	5	5.07	15.83	127.5	1.00	0.37	0.06	0.125	12.49	4.04	53.42	1850	200.31
0129R077	AL,X-65	4.65	5	4.96	15.0	124	0.96	0.343	0.0732	0.114	11.55	4.20	55.42	1773	216.12
0115R062	AL,X-65	4.65	5	4.96	15.0	127.5	1.02	0.394	0.0688	0.12	12.42	4.21	54.67	1833	212.61
1119R047	AL,X-65	4.65	5	5.05	14.73	120.0	1.01	0.40	0.07	0.109	11.24	4.24	55.99	1734	212.61
1011R023	AL,X-65	4.65	5	3.73	18.18	142.5	1.16	0.55	N/A	0.113	14.79	4.43	69.65	2083	226.67
1121R053	AL,X-65	7.00	5	5.68	15.02	142.5	0.92	0.33	0.06	0.089	11.66	6.50	79.36	2024	316.27
0117R065	1-5 micron	4.65	5	4.95	15.0	120.0	1.03	0.426	0.0558	0.102	12.44	3.29	60.56	1763	240.72
0131R080	1-5 micron	4.65	5	4.96	16.1	139	0.93	0.339	0.0604	0.09	12.49	3.50	78.12	1959	307.49
1119R045	1-5 micron	4.65	5	5.30	15.21	135.0	1.06	0.46	0.07	0.098	12.47	3.90	69.73	1916	288.16
1011R024	1-5 micron	4.65	5	4.75	17.66	151.2	1.05	0.46	N/A	0.085	14.34	4.20	94.74	2174	333.8
0116R063	3-4.5 micron	4.65	5	4.94	15.2	120.0	1.06	0.388	0.061	0.172	12.49	2.81	37.73	1761	189.77
1119R046	3-4.5 micron	4.65	5	5.89	15.58	135.0	0.99	0.40	0.07	0.089	12.49	3.85	77.31	1942	303.98
0116R064	3-4.5 micron	4.65	5	4.96	14.7	135.0	0.97	0.380	0.066	0.086	11.24	4.13	76.49	1887	314.52
0129R078	3-4.5 micron	4.65	5	4.97	15.0	132	0.92	0.331	0.0748	0.089	12.21	4.23	75.46	1903	296.95
0131R079	10-14 micron	4.65	5	4.97	15.0	89	1.22	0.361	0.0578	0.36	12.62	3.45	11.84	1281	35.14
0121R066	10-14 micron	4.65	5	4.98	15.0	97.5	1.15	0.391	0.0662	0.258	12.47	3.94	19.86	1445	57.98
1101R030	10-14 micron	4.65	5	5.12	14.92	101.2	1.04	0.29	0.07	0.246	12.39	4.25	21.38	1502	63.26
1101R031	10-14 micron	4.65	10	6.28	15.70	105.0	1.14	0.33	0.09	0.313	13.12	4.29	17.63	1556	45.68
1118R044	10-14 micron	4.65	5	5.01	15.56	110.0	1.18	0.40	0.06	0.279	12.53	4.37	21.19	1614	54.47
1024R026	10-14 micron	4.65	5	6.26	16.06	95.0	1.13	0.37	0.08	0.257	13.68	4.40	18.79	1411	57.98

Table 5.1.2: General Data Collection Sheet For Flakes

RUN NO	POWDER	MASS (gms)	FUSE (cm)	P_O (psia)	P_i (psia)	P_{max} (psia)	t@ P_{max} (sec)	t_v (sec)	t_{igs} Dur (sec)	t to P_{max} (sec)	Pfinal (psiA)	Effective mass(g)	dP/dt (avg)	T_{max}	dP/dt max
0307R098	200+325 mesh	4.18	5	4.97	15.0	124	1.16	0.425	0.0618	0.232	12.39	3.80	28.86	1824	205.58
0306R095	200+325 mesh	4.41	5	4.97	15.0	129	0.96	0.353	0.017	0.102	11.38	3.96	65.30	1877	275.86
1125R056	200+325 mesh	4.65	5	7.51	17.48	135.0	1.16	0.34	0.07	0.319	14.84	3.99	24.18	2000	137.1
0203R082	200+325 mesh	4.65	5	4.97	14.7	129	0.99	0.330	0.0648	0.154	11.24	4.06	14.15	1850	272.35
0127R071	200+325 mesh	4.65	5	4.96	14.8	131.2	1.08	0.379	0.0642	0.199	11.26	4.12	35.09	1897	272.35
0224R088	-325 mesh	3.5	5	4.98	15.4	105	1.19	0.410	0.0584	0.281	13.20	2.88	19.90	1573	80.83
0219R085	-325 mesh	4.18	5	4.96	15.0	114	1.12	0.396	0.0666	0.221	12.48	3.32	26.86	1679	87.85
0220R086	-325 mesh	4.41	5	4.96	15.0	124	1.00	0.351	0.0666	0.147	12.48	3.47	44.62	1833	251.27
0220R087	-325 mesh	4.65	5	4.97	15.0	119	1.01	0.316	0.0674	0.194	12.48	3.65	32.96	1752	135.30
1125R057	-325 mesh	4.65	5	7.22	16.3	132	0.99	0.321	0.064	0.169	13.73	3.73	42.67	1952	256.54
0129R076	-325 mesh	4.65	5	4.96	15.0	121	1.05	0.360	0.0636	0.184	12.48	3.77	35.33	1788	205.58
0127R073	-325 mesh	4.65	5	4.95	15.0	107.5	1.35	0.407	0.061	0.438	12.95	3.97	13.10	1577	57.98
0310R100	-90 mesh	4.18	5	4.96	15.0	120	1.13	0.435	0.066	0.191	12.43	3.56	34.06	1768	147.60
0306R097	-90 mesh	4.41	5	4.95	15.0	120	1.09	0.415	0.0172	0.174	12.34	3.80	36.35	1778	158.14
1126R060	-90 mesh	4.65	5	7.44	17.5	128.7	1.12	0.298	0.0628	0.317	14.91	3.91	21.93	1916	73.80
0123R070	-90 mesh	4.65	5	4.96	14.7	125.0	1.05	0.389	0.0662	0.159	11.25	3.97	41.35	1821	224.91
0203R081	-90 mesh	4.65	5	4.95	14.9	124	1.01	0.327	0.0756	0.179	11.52	4.02	37.72	1816	184.50
0307R099	20-120 mesh	4.18	5	4.95	15.0	116	1.14	0.391	0.068	0.25	12.47	3.57	25.23	1730	96.64
1127R061	20 - 120 mesh	4.65	5	10.27	21.0	127.5	1.49	0.364	0.07	0.623	17.34	3.79	11.31	1903	65.01
0306R096	20-120 mesh	4.41	5	4.95	14.9	125	1.10	0.481	0.0148	0.118	11.32	3.80	54.36	1824	228.42
0204R083	20-120 mesh	4.65	5	4.98	15.0	124	1.05	0.350	0.058	0.197	12.12	4.02	33.79	1805	191.52
0128R074	20-120 mesh	4.65	5	4.95	14.6	122.5	1.00	0.320	0.065	0.176	11.24	4.04	36.77	1795	209.09

The experimental values of dP/dt_{max} (Ψ=1) for all the material types investigated in this project are shown in Figure 5.1.1. For aluminum powders, a trend of a significantly higher rate of flame propagation for finer particle sizes is clear for all but the finest powder. A small decrease in the rate of flame propagation (dP/dt_{max}) was observed for the Al powder with nominal diameters of 3-4.5 μm by Alfa Aesar for which the BET diameter was found to be smaller than that for an Atlantic Equipment Engineers powder with nominal diameters of 1-5 μm (cf. Table 1). As noted above, the BET diameters for

all the Al flake types were significantly smaller than those for Al powders; however, the measured rates of pressure rise were relatively low. The change in the rate of pressure rise was also small between the different types of flakes. Large error bars, especially for the flakes of nominal size -325 Mesh, are indicative of a poor repeatability of the pressure traces between the experiments with the same type of flakes. Repeating experiments did enhance statistical data processing but did not eliminate vast discrepancy between the measured values of dP/dt_{max} from run to run.

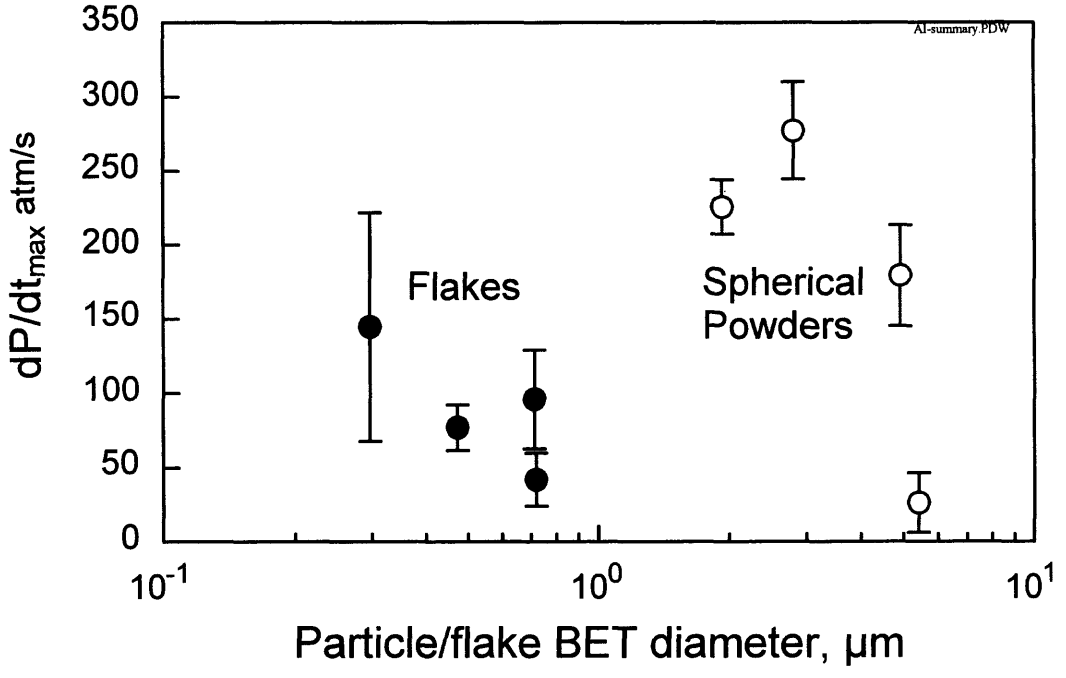

Figure 5.1.1: Comparison of Aluminum Powders and Flakes.

The following tables show the respective powders and flakes used for the comparison with their rate of pressure rise (dP/dt_{max}) and their respective equivalence ratios.

ALUMINUM POWDERS:

Table 5.1.3: Aluminum, 3-4.5 microns

BET diameter, micrometer	RUN NO	Equivalence Ratio	dP/dt max	Pmax/Pi	T_{max}	Pi/Pfinal
1.93	0116R063	0.90	189.77	7.88	1761	1.22
1.93	1119R046	1.20	303.98	8.66	1942	1.25
1.93	0116R064	1.36	314.52	9.15	1887	1.31
1.93	0129R078	1.37	296.95	8.84	1903	1.23

Table 5.1.4: Aluminum, 1-5 microns

BET diameter, micrometer	RUN NO	Equivalence Ratio	dP/dt max	Pmax/Pi	T_{max}	Pi/Pfinal
2.81	0131R080	1.06	307.49	8.62	1959	1.29
2.81	0117R065	1.07	240.72	8.01	1763	1.20
2.81	1011R024	1.16	333.8	8.56	2174	1.23
2.81	1119R045	1.25	288.16	8.87	1916	1.22

Table 5.1.5: Aluminum, X-65

BET diameter, micrometer	RUN NO	Equivalence Ratio	dP/dt max	Pmax/Pi	T_{max}	Pi/Pfinal
4.92	OCT7R019	0.59	40.41	5.80	1657	N/A
4.92	OCT7R018	0.69	19.33	4.92	1380	N/A
4.92	OCT4R014	1.01	159.90	7.20	2138	N/A
4.92	1011R023	1.18	226.67	7.84	2083	1.23
4.92	1120R049	1.24	200.31	8.05	1850	1.27
4.92	0115R062	1.36	212.61	8.49	1833	1.21
4.92	0129R077	1.36	216.12	8.27	1773	1.29
4.92	1119R047	1.40	212.61	8.14	1734	1.31
4.92	1121R053	2.10	316.28	9.48	2024	1.29

Table 5.1.6: Aluminum, 10-14 microns

BET diameter, micrometer	RUN NO	Equivalence Ratio	dP/dt max	Pmax/Pi	T_{max}	Pi/Pfinal
5.41	0131R079	1.12	35.14	5.92	1281	1.1880
5.41	0121R066	1.28	57.98	6.51	1445	1.2007
5.41	1024R026	1.33	57.98	5.91	1411	1.1741
5.41	1101R031	1.33	45.68	6.68	1556	1.1971
5.41	1118R044	1.36	54.47	7.07	1614	1.2426
5.41	1101R030	1.38	63.26	6.78	1502	1.2040

ALUMINUM FLAKES:

Table 5.1.7: Aluminum, 200+325 Mesh Flake

BET diameter, micrometer	RUN NO	Equivalence Ratio	dP/dt max	Pmax/Pi	T_{max}	Pi/Pfinal
0.47	1125R056	1.11	137.1	7.72	2000	1.18
0.47	0307R098	1.23	205.58	8.26	1824	1.21
0.47	0306R095	1.29	275.86	8.61	1877	1.31
0.47	0203R082	1.34	272.35	8.77	1850	1.31
0.47	0127R071	1.35	272.35	8.86	1897	1.32

Table 5.1.8: Aluminum, 20-120 Mesh Flake

BET diameter, micrometer	RUN NO	Equivalence Ratio	dP/dt max	Pmax/Pi	T_{max}	Pi/Pfinal
0.71	1127R061	0.88	65.01	6.08	1903	1.21
0.71	0307R099	1.16	96.64	7.74	1730	1.20
0.71	0306R096	1.24	228.42	8.39	1824	1.31
0.71	0204R083	1.31	191.52	8.27	1805	1.23
0.71	0128R074	1.34	209.09	8.39	1795	1.30

Table 5.1.9: Aluminum, -325 Mesh Flake

BET diameter, micrometer	RUN NO	Equivalence Ratio	dP/dt max	Pmax/Pi	T_{max}	Pi/Pfinal
0.3	0224R088	0.91	80.83	6.83	1573	1.16
0.3	0219R085	1.08	87.85	7.59	1679	1.20
0.3	1125R057	1.11	256.54	8.13	1952	1.19
0.3	0220R086	1.12	251.27	8.24	1833	1.20
0.3	0220R087	1.18	135.30	7.92	1752	1.20
0.3	0129R076	1.22	205.58	8.09	1788	1.20
0.3	0127R073	1.28	57.98	7.16	1577	1.16

Table 5.1.10: Aluminum, -90 Mesh Flake

BET diameter, micrometer	RUN NO	Equivalence Ratio	dP/dt max	Pmax/Pi	T_{max}	Pi/Pfinal
0.72	1126R060	1.09	73.80	7.36	1916	1.17
0.72	0310R100	1.15	147.60	8.00	1768	1.21
0.72	0306R097	1.23	158.14	8.01	1778	1.21
0.72	0123R070	1.31	224.91	8.48	1821	1.31
0.72	0203R081	1.31	184.50	8.28	1816	1.30

As mentioned before the burn rate corresponding to equivalence ratio of 1 is found for each of the powders and flakes for comparison (Figure 4.2.1 and Figure 4.2.2). The plots show that dP/dt_{max} increases with equivalence ratio and this increase is stronger for powders than flakes. Also overall rates are higher for spherical powders.

Comparison of powders versus flakes (Figure 5.1.1) shows that generally higher rates of pressure rise and, thus, of flame propagation, are achieved with aluminum powders with nominal sizes in the general range of 1 – 10 μm. The comparison shows a higher burn rate for powders than flakes except for the very coarse spherical powder.

This observation was supported by the measurements of the final pressure in the explosion vessel. Analogous to the data processing for the dP/dt_{max} measurements, a linear fit for the experimental pressure ratio as a function of equivalence ratio, Ψ, was found for each type of material. The resulting values of the pressure ratios implied by the linear fit at Ψ=1 are shown in Figure 5.1.2 for both flakes and particles with the error bar showing the standard deviation of experimental points from the found linear fit.

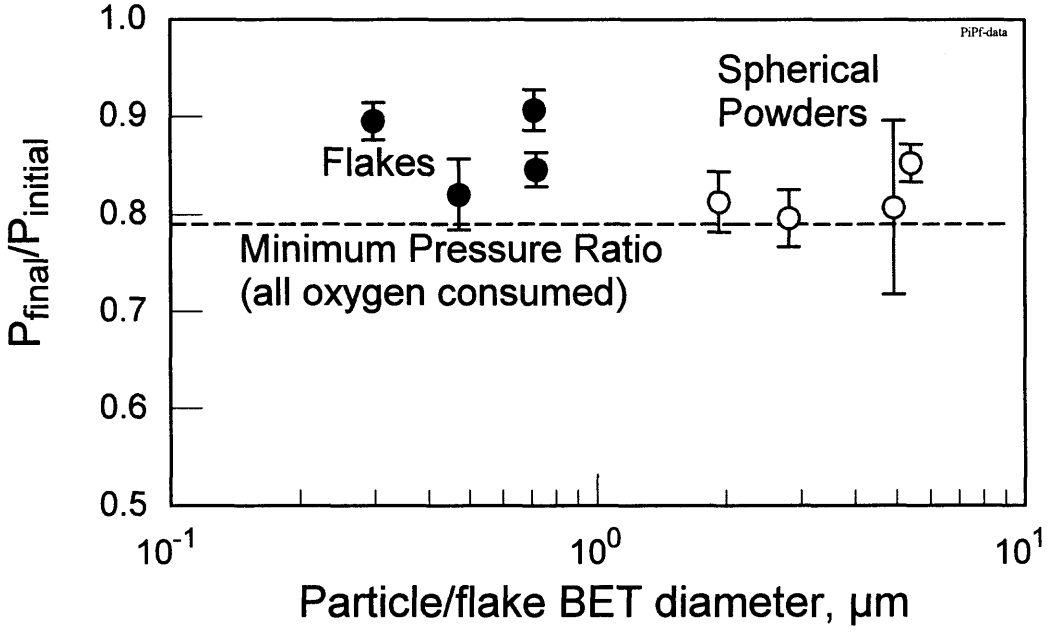

Figure 5.1.2: Combustion Completeness of Aluminum Powders and Flakes Based on Ratio of Final Pressure to Initial Pressure.

For experiments conducted at Ψ=1 or greater, all the available oxygen should be consumed in case of complete combustion. For air containing 21 mole % of O_2 and used as the only oxidizer in these experiments, the minimum final pressure ratio to the initial pressure should, therefore, be equal to (1-0.21)/1=0.79. Comparing the experimental pressure ratios shown in Figure 5.1.2, one can see that indeed the combustion of finer aluminum powders was more complete than that of flakes. Also in agreement with very

low values of dP/dt_{max} for the coarser aluminum powder, the respective pressure ratio is fairly high, showing rather incomplete combustion.

Combustion product phase analysis based on x-ray diffraction patterns was conducted for selected samples (Figure 5.1.3) of each of the material types. The observed patterns were compared to reference patterns from the PDF-2 database (Powder Diffraction File (PDF-2), Joint Committee for Powder Diffraction, Standards International Center for Diffraction Data, Newtown Square, PA, U.S.A.)

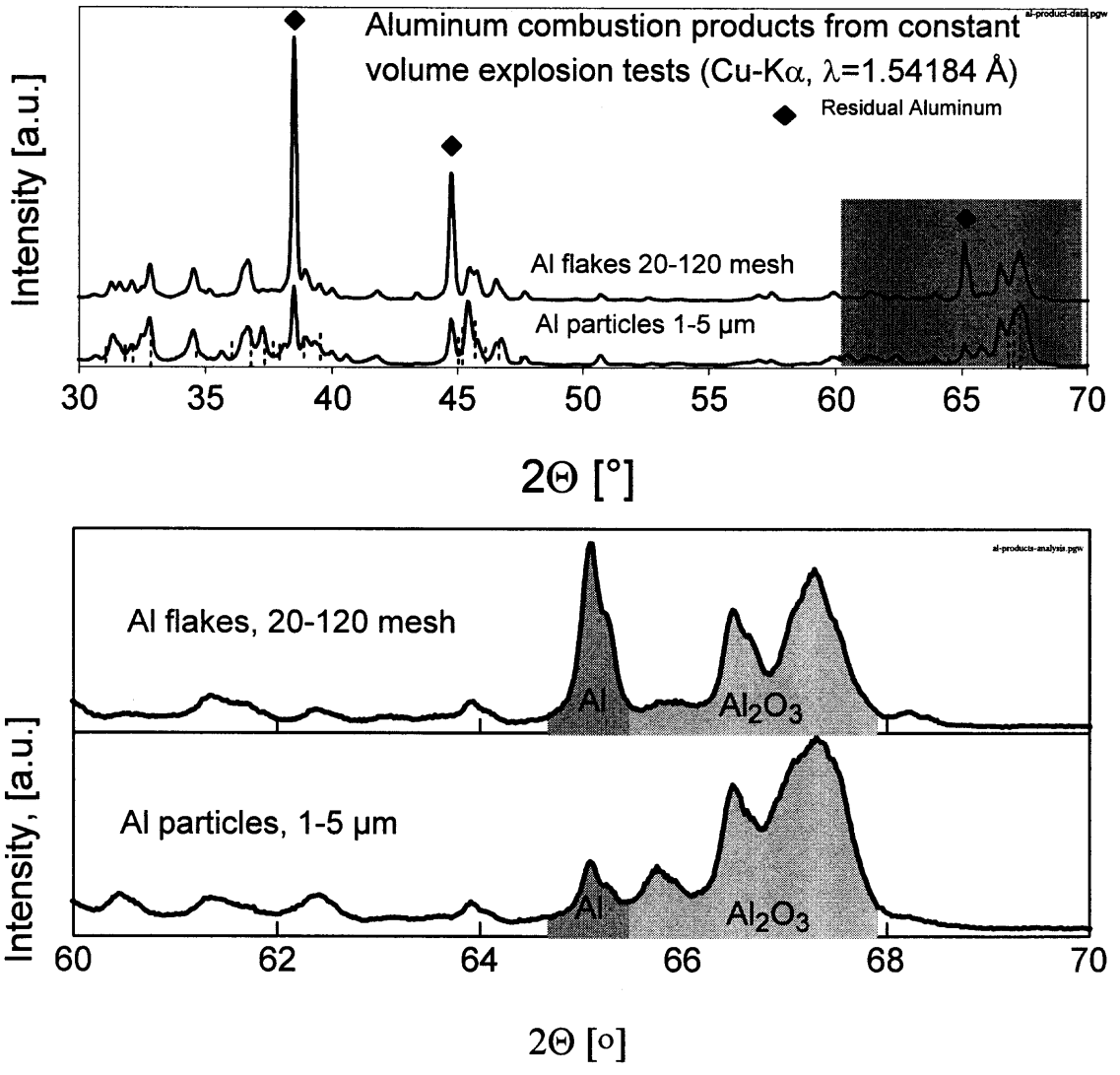

Figure 5.1.3: X-ray Diffraction Patterns of Two Representative Combustion Products. [Aluminum peaks are marked with solid diamonds; vertical dashed lines show the peak positions of δ-Al_2O_3 (PDF-2 database, reference card 46-1131)]

In addition to diffraction peaks of residual Al, peaks roughly consistent with spinel-like aluminum oxides or oxynitrides are observed in the diffraction patterns. Although a number of structurally similar oxides or oxynitrides could be matched against the measured patterns with equal success, a perfect match was not achieved. It is

expected that the combustion products consist of disordered oxide phases with at least traces of nitrogen. A more detailed analysis is needed to determine structure and composition of the oxide products of Al combustion in the present experiment. To assess the degree of conversion of the combustion, the ratio of integrated intensities of Al and Al oxide diffraction peaks was used as a semi quantitative measure. In the absence of detailed structural information, the diffraction peaks in the vicinity of the 100%-reflection of δ-Al_2O_3 were summarily integrated from 65.5 ° to 68.5 ° 2Θ and set in proportion to the 220 peak of Al at 65.19 ° 2Θ. The results of this comparison are shown in Figure 5.1.4; as expected these estimates mirror well the ratios of initial to final pressures (Figure 5.1.2).

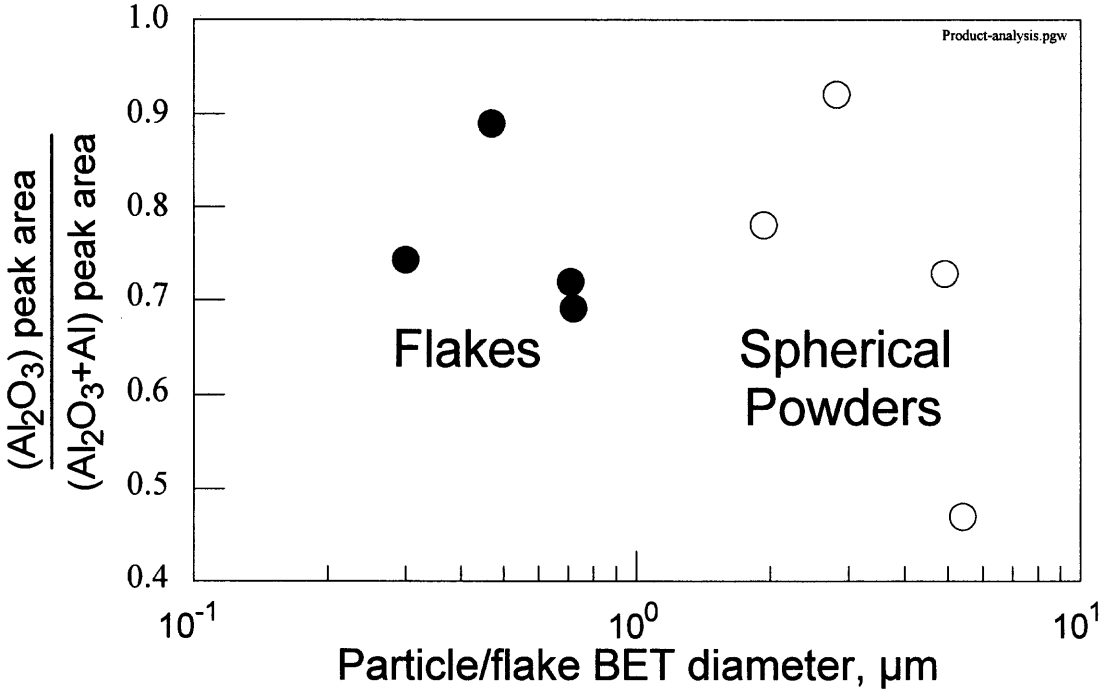

Figure 5.1.4: Semiquantitative Comparison of Combustion Completeness, Estimated via Integrated Intensities of Al and Al oxides Obtained from X-ray Diffraction Patterns of Combustion Products.

5.2 Discussion

The observed trend of the less complete and slower combustion for the aluminum flakes as compared to regular, micro-sized aluminum powders is somewhat unexpected. As noted above, very thin flakes with highly developed specific surface should react faster during heterogeneous reactions at relatively low temperatures typical of aluminum ignition. Based on the measured BET diameters, it was also expected that upon ignition, molten droplets formed from individual flakes would be smaller than molten aluminum particles. Therefore, faster ignition and combustion rates for the flakes would seem reasonable. However, the above arguments do not consider dramatic differences in the behavior of spherical particles and flakes in gas flows. While detailed analysis of these fluid mechanics problems is outside the scope of this project, it is clear that flakes could readily induce local swirls and create their own flow patterns, while fine particles tend to follow the gas flow. Producing local swirling patterns could result in significant agglomeration of the flakes prior to their ignition. Such an agglomeration could be one of the reasons of relatively slow and incomplete combustion observed in this work. Additional experiments or theoretical analyses would be needed to further elucidate the effects of such flake/gas flow interaction effects on the rate of combustion of aerosolized flakes.

CHAPTER 6

CONCLUSION

Combustion rates of aerosolized in air spherical aluminum particles and flakes are measured and compared to each other. Constant volume explosion technique was used for combustion experiments. Even though the BET diameters of all the tested aluminum flake samples were less than respective BET diameters for spherical aluminum particles, both the combustion rates and reaction completeness were higher for the particles with mean diameters (based on volume distribution) of up to 10 μm. This conclusion is based on comparisons of the rates of pressure rise, consumption of oxygen from the air in the vessel, and completeness of the aluminum conversion to oxide based on the analyses of the condensed combustion products. It is speculated that the relatively slow rate of combustion and incomplete reaction observed for flakes are due to agglomeration of flakes before their ignition within the small scale eddies produced as a result of flakes interaction with the gas flows induced by the propagating flame.

REFERENCES

1 Cashdollar, K.L. (1994) Flammability of metals and other elemental dust clouds. Process Safety Progress 13(3), pp. 139-45.

2 Hertzberg, M., Zlochower, I.A., and Cashdollar, K.L., (1992) Metal dust combustion: explosion limits, pressures, and temperatures. Proceedings of The Combustion Institute, 24, pp. 1827-1835.

3 Mench, M. M., Kuo, K. K., Yeh, C. L., and Lu, Y. C. (1998) Comparison of thermal behavior of regular and ultra-fine aluminum powders (Alex) made from plasma explosion process. Combustion Science and Technology, 135 (1-6), pp. 269-292.

4 Pranda, P., Prandova, K., and Hlavacek, V. (2000) Particle size and reactivity of aluminum powders. Combustion Science and Technology, 156, pp. 81-96.

5 Schoenitz, M., Dreizin, E.L., and Shtessel, E., (2003) Constant volume explosions of aerosols of metallic mechanical alloys and powder blends. Journal of Propulsion and Power, 19(3), pp. 405-412.